Journal of Materials Chemistry B

COMMUNICATION

View Article Online
View Journal | View Issue

Gas-phase self-assembly of soft nanocomposites for efficient gene transfection and photothermal therapy†

Cite this: *J. Mater. Chem. B*, 2014, **2**, 3185

Received 19th February 2014
Accepted 16th March 2014

DOI: 10.1039/c4tb00271g

www.rsc.org/MaterialsB

Jeong Hoon Byeon*[a] and Young-Woo Kim*[b]

The gene transfection efficiency of Au@PDMS–PLL soft nanocomposites was higher than those of SiO_2–PLL and PEI; and moreover, the nanocomposites did not show significant cell cytotoxicity in *in vitro* measurements. The soft nanocomposites were also sensitive during photothermal therapy with infrared light, which produced a cytotoxic effect on the targeted HeLa cells.

Nanocomposites of inorganic materials in polymer matrices have attracted a great deal of attention because of their wide applications as biosensors, optical devices, micromechanical devices, and advanced catalytic membranes.[1] Gold (Au) nanoparticles, an inorganic material, have attracted widespread and rapidly increasing interest because of their unique physical, chemical, and biocompatible properties, as well as promising applications in catalysis and sensing.[2] Hence, incorporation of Au nanoparticles with polymeric components as nanocomposites has also attracted enormous interest in both the science and technology fields.[3] There are many recent reports of Au nanoparticles@polymer nanocomposites that use the optical properties of nanoparticles to obtain effects such as wavelength-tunable light attenuation, chemically tunable luminescence, surface plasmon resonance, and lasing.[4]

The usual route to synthesize Au@polymer nanocomposites is wet chemistry; however, the synthesis method involves multiple steps, and most nanoparticles are located at the surface only.[3] In contrast to classical wet chemical methods, gas-phase processing involves far fewer preparation steps.[5] It also produces materials continuously, allowing for straightforward collection of particles and the generation of low waste.[6] Nevertheless, conventional gas-phase synthesis typically requires high temperatures (>2000 K), and can only be used to fabricate or deposit metallic nanoparticles.[7] Such high temperatures can induce decomposition of polymeric/organic components. For this reason, the current gas-phase equivalent of a one-pot approach is not a viable strategy for synthesizing biocompatible nanocomposites without expensive and time-consuming post-functionalization steps.[8]

In this work, Au@polymer nanocomposites were synthesized "on the fly" in a serial gas-phase reactor (Scheme S1†). Spark-produced Au nanoparticles[9] (3 L min^{-1}, N_2 gas) passed over a collison atomizer [containing 750 mg of polydimethylsiloxane (PDMS)–250 mg of poly-L-lysine (PLL) in 100 mL of dichloromethane (DCM)] orifice where they mixed with atomized PDMS–PLL to form hybrid droplets. The droplets then passed through a heated tubular flow reactor containing silica gels and activated carbons operating at a 90 °C wall temperature to drive DCM from the droplets, resulting in PDMS–PLL capped Au nanoparticles, *i.e.*, Au@PDMS–PLL nanocomposites. The choice of polymer plays an important role in determining the functionality of the nanocomposites. In this context, PDMS is an attractive polymer matrix due to its many favorable properties such as chemical inertness, biocompatibility, mechanical flexibility and stability, optical clarity in the visible and ultraviolet region, and most importantly, its ease of processing.[10] Moreover, PLL is a polypeptide with amino acid lysine as a repeat unit and is biodegradable. This is one of the first cationic polymers used for gene delivery due to its low immunogenicity, the capacity to deliver large gene payloads, its stability, and the ease of passage for the gene molecules through cell membranes.[11]

The purpose of the present work is to report the synthesis of Au@PDMS–PLL nanocomposites using gas-phase self-assembly. In this work, the applicability and suitability of these composites as both nanocarriers for gene delivery and nanoheaters for photothermal therapy were explored since the resultant materials show restructured Au [active in surface plasmon resonance (SPR) heating] and PLL functionalization (inducing positive surface charge) in the gas-phase is not a critical issue.[11] Gene delivery to cure diseases, which is difficult

[a]*Department of Chemistry, Purdue University, Indiana 47907, USA. E-mail: jbyeon@purdue.edu; Tel: +1 765 494 5499*

[b]*Department of Automotive Engineering, Hoseo University, Asan 336-795, Republic of Korea. E-mail: ywkim@hoseo.edu; Tel: +82 41 540 5819*

† Electronic supplementary information (ESI) available. See DOI: 10.1039/c4tb00271g

to achieve by traditional clinical methods, has been actively pursued for decades.[11] Many formulations of polymer-based nanocarriers exist as colloidal liquids, usually synthesized using time-consuming batch wet chemical processes and generally stable only for short periods of time. Also, some polymer systems are specifically designed to be gradually degradable by hydrolysis, making long-term storage in liquid form not a viable option. One approach for overcoming such stability limitations is to formulate and store dry powders from a gas-phase preparation.[8] Photothermal therapy uses a nanoheater, which is excited with specific band light. This activation brings the heater to an excited state where it then releases vibrational energy (heat), and this heat is the actual method of therapy that kills the targeted cells.[12] The major challenge in these applications, however, is to develop safe and efficient nanocarriers and nanoheaters for these biomedical purposes, in which nanomaterials are usually involved.[13] Although much progress has been reported regarding the use of polymeric/organic components with various hard nanomaterials, such as carbon nanotubes, silica nanoparticles, metallic nanostructures,[14] a lot more effort (*i.e.* flexible nanocomposites such as graphene or nanogel platform based)[13] is still required to develop more efficiency for potential gene and photothermal therapy.

Results and discussion

Fig. 1 summarizes the results of the size distributions of Au, the atomized PDMS–PLL solution, and the merged particles (Au@PDMS–PLL). The total number concentration (TNC), geometric mean diameter (GMD), and geometric standard deviation (GSD) of the Au@PDMS–PLL nanocomposites are 1.10×10^7 particles per cm^3, 59.4 nm, and 1.58, respectively. The same data for pure Au nanoparticles are 0.96×10^7 particles per cm^3, 18.0 nm, and 1.50, respectively, and for the atomized PDMS–PLL solutions are 0.77×10^7 particles per cm^3, 44.5 nm, and 1.60, respectively (also shown in Table SI†). The size distribution of the Au@PDMS–PLL is similar to that of the atomized PDMS–PLL particles. This implies that nearly quantitative incorporation of the Au nanoparticles into the PDMS–PLL particles may be possible at this configuration.

Fig. 2 shows representative low- and high-magnification TEM images of collected Au and PDMS–PLL nanoparticles, and Au@PDMS–PLL nanocomposites. The TEM images reveal that the Au nanoparticles (left image) were agglomerates of several primary particles (each ~3.4 nm in diameter). Gaps between primary Au particles might have originated from impaction between the Au agglomerates and the TEM grid surface. The kinetic energy of the Au agglomerates directing onto the surface by electrostatic attraction is $\sim 10^{-19}$ J, which is smaller than those ($>5 \times 10^{-18}$ J) in previous reports for initiating fragmentation of aerosol agglomerates during impaction on a surface.[15] This implies that the agglomerates in the gas-phase consisted of weakly coherent primary Au particles (since most spark produced metallic particles were naturally positively charged due to energetic electron bombardment),[16] which could easily fragment upon the electrostatic sampling. The PDMS–PLL particles (middle image) have roughly spherical shapes and they are well separated. The particles exhibit boundaries between a core (dark, dense solid) section and a shell (bright, light solid) section. The formation of the spherical particles is attributed to the slow convective drying rate, for which the time for liquid evaporation was greater than the time required for supersaturated particles at a liquid–vapor interface to migrate back toward the droplet center. When the Au nanoparticles passed over the orifice of the atomizer (right image), it was clear that dark nanodots (since Au has a higher electron density and allows the transmission of fewer electrons compared to PDMS–PLL particles) were capsulated by PDMS–PLL components, which confirms that the Au@PDMS–PLL nanocomposites have been successfully synthesized. The mean mode diameters of the Au and the PDMS–PLL particles are 20 ± 5.1 nm and 49 ± 5.2 nm, respectively. The diameter slightly increased to 51 ± 3.8 nm after the incorporation. The increase of the Au nanoparticle size may have originated in part from coalescence between the PDMS–PLL encapsulated Au nanoparticles during heat treatment (due to thermal agglomeration). An average thickness of the PDMS–PLL layer on primary Au particles was 3.9 ± 1.6 nm, and another inset of the Au@PDMS–PLL further confirms the incorporation of the PDMS–PLL layer on primary Au particles. The morphologies of the Au@PDMS–PLL are different from those of individual Au and PDMS–PLL particles. Specifically, the spherical shapes of primary Au particles in

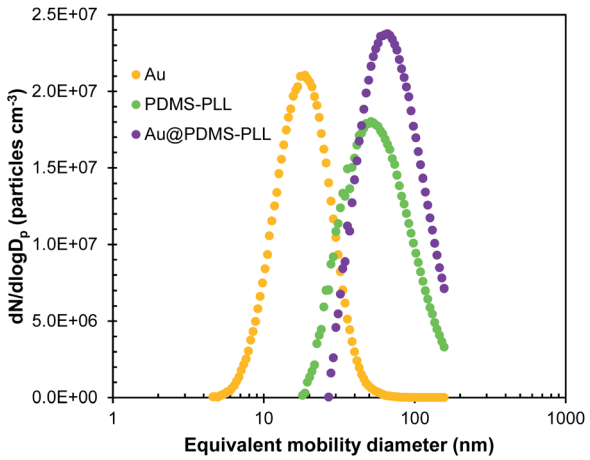

Fig. 1 Size distributions of spark produced Au and collison atomized PDMS–PLL nanoparticles, and their incorporated structure (Au@PDMS–PLL) through gas-phase self-assembly.

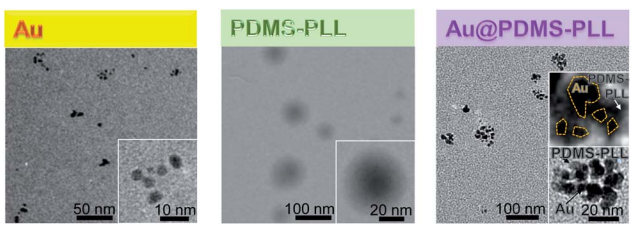

Fig. 2 Low and high magnification TEM images of gas-phase self-assembled Au, PDMS–PLL, and merged (Au@PDMS–PLL) samples.

agglomerate evolved to more irregular shapes through the incorporation with PDMS–PLL, and the particle surfaces became more corrugated (see an inset of the Au@PDMS–PLL in Fig. 2). The production yield of Au@PDMS–PLL from gas-phase self-assembly is approximately 91.8%. The yield was determined by the area fraction of Au@PDMS–PLL-to-all particles in the TEM image.

Fig. S1a (ESI†) shows the UV-vis spectra of Au@PDMS–PLL nanocomposites including individual Au and PDMS–PLL particles. PDMS–PLL did not show any absorbance in the visible region whereas Au@PDMS–PLL had a broad absorbance centered at ~550 nm.[17] This absorbance was due to the surface plasmon excitation of Au nanoparticles (~530 nm)[18] and confirmed the Au incorporation with the PDMS component. The incorporation of PDMS–PLL on Au nanoparticles was further investigated by Fourier transform infrared (FTIR) spectroscopy (Fig. S1b, ESI†). Both Au@PDMS and Au@PDMS–PLL samples show that characteristic bands of the CH_3 bend, CH_2 bend, and Si–O–Si stretching of PDMS are respectively found at around 2960, 2945, and 1050 cm^{-1}.[19] For Au@PDMS–PLL, it can also be seen that the vibration of amide I appeared at ~1646 cm^{-1}, amide II was observed at ~1537 cm^{-1}, and that of free amino groups (NH stretching vibrations) was noticed at ~3050 cm^{-1},[20] which confirms the further conjunction with PLL on Au@PDMS. Fig. S1 (ESI†) also noted zeta potential data of Au@PDMS and Au@PDMS–PLL samples at pH 7.3. The anionic surface (−17 mV) was transferred to cationic polarity (+6 mV) by incorporating PLL, which implies that the nanocomposites can electrostatically interact with negatively charged plasmid DNA (pDNA). The zeta potential of nanocomposites after pDNA complexing was +3.7 mV. The difference in zeta potential between nanocomposites and the pDNA complexes may originate from negatively charged DNA due to the phosphate ions loaded on the outer surface of the composites.

We tested the cytotoxicity of the Au@PDMS–PLL nanocomposites as a potential material for biomedical applications. HeLa cells were incubated with the nanocomposites for 24 h, and cell viability was determined by a standard MTT [3-(4,5-dimethylthiazol-2-yl)-diphenyltetrazolium bromide] assay (Fig. S2, ESI†). The fabricated nanocomposites were detached from the polytetrafluoroethylene substrate by immersing the samples in water and subjecting them to ultrasound treatment for 10 s. The results show that cell viability was more than 95% for the nanocomposites without infrared (IR) light. The cell viability was comparable with that obtained using SiO_2@PLL, and significantly higher than those from PEI. This implies that the gas-phase self-assembled nanocomposites warrant further investigation.

We next examined the ability of the merged particles to transfect HeLa cells using pDNA that contain the luciferase and enhanced green fluorescent protein (EGFP) gene. The transfection efficiency of pDNA in the cell line was the lowest due to the absence of its carriers (Fig. 3). We employed polyethyleneimine (PEI) and SiO_2@PLL as comparators since PEI is one of the widely employed transfection agents while SiO_2 would be a harder silicon-based biocompatible material for appropriate comparison with the elastic particles (containing

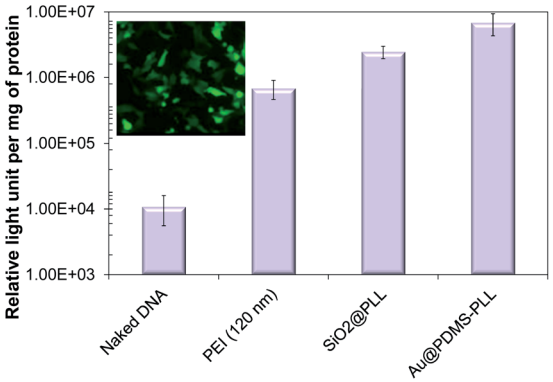

Fig. 3 *In vitro* measurements of gene transfection efficiency of Au@PDMS–PLL nanocomposites including naked DNA, PEI, and SiO_2@PLL reference samples. A fluorescence microscopy image of Au@PDMS–PLL–EGFP complexes is also displayed.

PDMS). The efficiency of the nanocomposites was the highest, even higher than that of PEI (also fabricated *via* collison atomization of 250 mg of PEI in 100 mL of DCM) and SiO_2@PLL. A lower transfection efficiency of the PEI than that of wet chemically prepared PEI (8.6×10^5 RLU mg^{-1}) may originate from the difference in their preparation. The SiO_2@PLL was tested as a reference representing harder nanocarriers than Au@PDMS–PLL nanocomposites. The inset in Fig. 3 shows the fluorescence of the HeLa cells for the Au@PDMS–PLL nanocomposites derived from EGFP expression, which further confirmed the transfection. Various factors and characteristics of nanomaterials could influence their transfectivity into cells. One of the important parameters that could affect the transfectivity of nanomaterials is their size.[21] We measured particle sizes using a zetasizer (Nano Z, Malvern Instruments, UK) with a liquid flow conditioner (MPT-2, Malvern Instruments, UK) to verify differences in hydrodynamic diameter between the particles. The hydrodynamic diameters of the SiO_2@PLL, SiO_2@PDMS–PLL, and Au@PDMS–PLL were 56.4 ± 5.3, 50.2 ± 6.6, and 42 ± 4.1 nm, respectively, although their sizes in the gas-phase were the same, 49 nm. The soft structure has a relatively small density (~1.1 g cm^{-3} for Au@PDMS–PLL *vs.* ~2.5 g cm^{-3} for SiO_2–PLL, ESI†), which may affect the differences in hydrodynamic diameter. Representative scanning probe microscopy (SPM) images are shown in Fig. 4, where the PDMS incorporated nanocomposites showed a less homogeneous shape than that of the SiO_2@PLL case. An elastic PDMS overlayer on the Au and SiO_2 nanoparticles could induce a larger

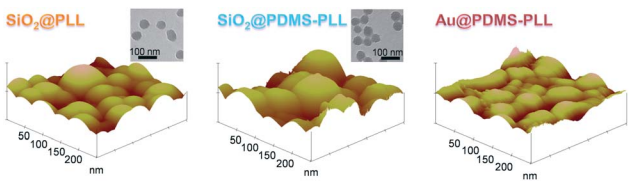

Fig. 4 3D topographs of the SiO_2@PLL, SiO_2@PDMS–PLL, and Au@PDMS–PLL nanocomposites.

aspect ratio of their final morphologies, as noted in SPM images. Therefore, the size of the Au@PDMS–PLL nanocomposites is relatively small compared to that of the SiO_2–PLL at the cell membrane in the liquid phase although their lateral dimensions are the same, resulting in a higher transfection efficiency.

In order to investigate the potential of the self-assembled Au@PDMS–PLL nanocomposites as nanoheaters, suspensions of the nanocomposites in agar were irradiated with 705 nm IR light emitted by a continuous wave laser (Scheme S1†). This wavelength was chosen since it was relatively close to the peak value of the Au@PDMS–PLL nanocomposites determined by UV-vis spectroscopy (Fig. S1a, ESI†). Even though there was no significant shift in the surface plasmon resonance (SPR) band, the obvious broadening in the SPR band has been shown after PDMS–PLL incorporation. The agar phantom was used to mimic physiological conditions. We observed an increase in temperature of the medium in the presence of IR radiation using an IR thermometer. Fig. S3 (ESI†) shows the change in temperature (ΔT) of the agar gels containing the Au@PDMS–PLL nanocomposites (10, 50, and 90 μg mL^{-1}); ΔT takes into account any temperature change in the control sample. The maximum value of ΔT (35.3 °C) was observed at the highest concentration (90 μg mL^{-1}) and longest exposure duration (90 s). The results indicated that the Au@PDMS–PLL nanocomposites could absorb visible light and rapidly convert the light energy to heat. This thermal energy on the surface of the nanocomposites could transfer to the medium due to microscopic temperature gradient between the composites and the media,[22] which finally induced macroscopic temperature increases (Fig. S3, ESI†). The equation can be solved analytically in the steady-state regime, yielding a maximum temperature located at the surface of the nanocomposite:[23]

$$\Delta T(D_n) = \frac{V_n P_{abs}}{2\pi k_0 D_n} \quad (1)$$

where D_n is the diameter of the nanocomposites, V_n is the volume of the nanocomposites, k_0 is the thermal conductivity of the surrounding liquid, and P_{abs} is the local light induced heating of the nanocomposite. In order to confirm briefly the feasibility of the nanocomposites in photothermal therapy, adenosine triphosphate (ATP) assay was further employed. It is well known that most cancer cells depend on glycolysis for ATP generation.[24] To confirm this, the HeLa cell line was used to test whether Au@PDMS–PLL under IR irradiation could inhibit ATP production. Several dark dots (inset of Fig. 5) over the cell indicate the presence of the nanocomposite. These composites appear to be mostly inside the cell rather than on the cell surface. It was found that in the presence of the nanocomposites in the culture medium, the IR laser radiation depleted ATP production (which can also be verified using fluorescence microscopy, as shown at the top of Fig. 5) while in the absence of the nanocomposites, the laser radiation did not affect the inhibition of ATP production. It may be suggested that the light energy delivered to the cell promotes the nanocomposites to an electronically excited state from which heat is generated *via* energy transfer processes.[12] As a result, irreversible thermo/chemical modifications of a variety of cell constituents are induced.

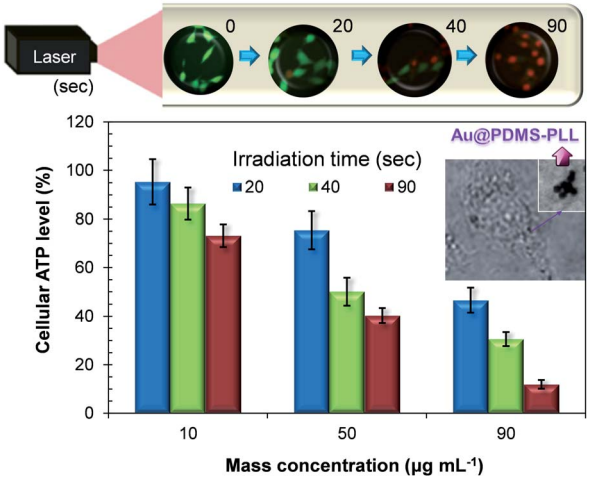

Fig. 5 ATP levels with different laser irradiation times (20–90 s) on Au@PDMS–PLL nanocomposites for different mass concentrations ranging from 10–90 μg mL^{-1}. Representative fluorescence images for different laser irradiation stages are also displayed. Green fluorescence indicates viable cells while red indicates dead cells.

Conclusions

For the first time, gas-phase self-assembly has been used to construct Au@PDMS–PLL soft nanocomposites without complex chemical preparation steps. The soft structure of the assembled Au@PDMS–PLL nanocomposites could be made biocompatible and suitable for linking efficient gene transfection and photothermal therapy. Further studies of *in vivo* distribution and photothermal effects are in progress. These results further establish low-temperature gas-phase processing as an efficient, scalable, and generalizable method for designing and fabricating an extraordinary broad range of functionalized nanobiomaterials.

Experimental summary

As shown in Scheme S1,† ambient spark discharge was selected in the present work for generation of Au nanoparticles as a convenient platform. The spark discharge is a kind of atmospheric pressure nonequilibrium discharge. The particle-laden flow was employed as the operating gas for atomizing the PDMS–PLL solution. The Au particle-laden flow passed over the atomizer orifice, where they mixed with atomized PDMS–PLL droplets to form hybrid droplets. The droplets then passed through a heated tubular reactor operating at 90 °C wall temperature to drive solvent from the droplets. The hybrid droplets were dried to yield Au@PDMS–PLL nanocomposites in the tubular reactor.

Acknowledgements

This research was supported by the Academic Research Fund of Hoseo University in 2013 (2013-0315).

Notes and references

1 A. Goyal, A. Kumar, P. K. Patra, S. Mahendra, S. Tabatabaei, P. J. J. Alvarez, G. John and P. M. Ajayan, *Macromol. Rapid Commun.*, 2009, **30**, 1116.
2 (*a*) H. Jia, X. Bai, N. Li, L. Yu and L. Zheng, *CrystEngComm*, 2011, **13**, 6179; (*b*) J. Nam, N. Won, H. Jin, H. Chung and S. Kim, *J. Am. Chem. Soc.*, 2009, **131**, 13639.
3 Q. Zhang, J.-J. Xu, Y. Liu and H.-Y. Chen, *Lab Chip*, 2008, **8**, 352.
4 A. Scott, R. Gupta and G. U. Kulkarni, *Macromol. Chem. Phys.*, 2010, **211**, 1640.
5 S. P. Shields, V. N. Richards and W. E. Buhro, *Chem. Mater.*, 2010, **22**, 3212.
6 S. E. Pratsinis, *AIChE J.*, 2010, **56**, 3028.
7 (*a*) E. Thimsen, *Chem. Mater.*, 2011, **23**, 4612; (*b*) S. H. Huh, D. H. Riu, Y. Naono, Y. Taguchi, S. Kawabata and A. Nakajima, *Appl. Phys. Lett.*, 2007, **91**, 093118; (*c*) R. G. Palgrave and I. P. Parkin, *J. Am. Chem. Soc.*, 2006, **128**, 1587.
8 (*a*) J. H. Byeon and J. T. Roberts, *ACS Appl. Mater. Interfaces*, 2012, **4**, 2693; (*b*) J. H. Byeon and Y.-W. Kim, *RSC Adv.*, 2013, **3**, 13685; (*c*) J. H. Byeon and Y.-W. Kim, *Chem. Eng. J.*, 2013, **229**, 540.
9 (*a*) J. H. Byeon, J. H. Park and J. Hwang, *J. Aerosol Sci.*, 2008, **39**, 888; (*b*) J. H. Byeon and J.-W. Kim, *Thin Solid Films*, 2010, **519**, 700.
10 (*a*) J. N. Lee, C. Park and G. M. Whitesides, *Anal. Chem.*, 2003, **75**, 6544; (*b*) D. Li, C. Li, A. Wang, Q. He and J. Li, *J. Mater. Chem.*, 2010, **20**, 7782.
11 (*a*) Y. Zhu, W. Meng, H. Gao and N. Hanagata, *J. Phys. Chem. C*, 2011, **115**, 13630; (*b*) L. Marsich, A. Bonifacio, S. Mandal, S. Krol, C. Beleites and V. Sergo, *Langmuir*, 2012, **28**, 13166; (*c*) J. H. Byeon, H.-K. Kim and J. T. Roberts, *Macromol. Rapid Commun.*, 2012, **33**, 1840; (*d*) J. H. Byeon and J. T. Roberts, *Chem. Mater.*, 2012, **24**, 3544.
12 (*a*) Ž. Krpetić, P. Nativo, V. Sée, I. A. Prior, M. Brust and M. Volk, *Nano Lett.*, 2010, **10**, 4549; (*b*) A. F. Zedan, S. Moussa, J. Terner, G. Atkinson and M. S. El-Shall, *ACS Nano*, 2013, **7**, 627; (*c*) Z. Zha, X. Yue, Q. Ren and Z. Dai, *Adv. Mater.*, 2013, **25**, 777.
13 L. Feng, S. Zhang and Z. Liu, *Nanoscale*, 2011, **3**, 1252.
14 (*a*) K. Yang, L. Feng, X. Shi and Z. Liu, *Chem. Soc. Rev.*, 2013, **42**, 530; (*b*) C.-H. Wang, C.-W. Chang and C.-A. Peng, *J. Nanopart. Res.*, 2011, **13**, 2749.
15 (*a*) S. Rothenbacher, A. Messerer and G. Kasper, *Part. Fibre Toxicol.*, 2008, **5**, 9; (*b*) S. Froeschke, S. Kohler, A. P. Weber and G. Kasper, *J. Aerosol Sci.*, 2003, **34**, 275.
16 J. H. Byeon and J.-W. Kim, *Langmuir*, 2010, **26**, 11928.
17 (*a*) M. Kahraman, P. Doggumati, O. Kurtulus, E. Seker and S. Wachsmann-Hogiu, *Sci. Rep.*, 2013, **3**, 3396; (*b*) S. Lee, H.-J. Shin, S.-M. Yoon, D. K. Yi, J.-Y. Choi and U. Paik, *J. Mater. Chem.*, 2008, **18**, 1751; (*c*) H. SadAbadi, S. Badilescu, M. Packirisamy and R. Wüthrich, *J. Nanosci. Nanotechnol.*, 2013, **13**, 6880.
18 A. V. Deore, V. N. Bhoraskar and S. D. Dhole, *Radiat. Phys. Chem.*, 2014, **96**, 97.
19 R. Gupta and G. U. Kulkarni, *ChemSusChem*, 2011, **4**, 737.
20 J.-B. Kim, T. Premkumar, O. Giani, J.-J. Robin, F. Schue and K. E. Geckeler, *Macromol. Rapid Commun.*, 2007, **28**, 767.
21 S. Prabha, W.-Z. Zhou, J. Panyam and V. Labhasetwar, *Int. J. Pharm.*, 2002, **244**, 105.
22 H. H. Richardson, M. T. Carlson, P. J. Tandler, P. Hernandez and A. O. Govorov, *Nano Lett.*, 2009, **9**, 1139.
23 O. Neumann, A. S. Urban, J. Day, S. Lal, P. Nordlander and N. J. Halas, *ACS Nano*, 2013, **7**, 42–49.
24 H. Huang, N. Liu, H. Guo, S. Liao, X. Li, C. Yang, S. Liu, W. Song, C. Liu, L. Guan, B. Li, L. Xu, C. Zhang, X. Wang, Q. P. Dou and J. Liu, *PLoS One*, 2012, **7**, e49062.